Bayesian integrated equilibrium reconstruction at WEST using magnetic, density and temperature diagnostics

J. De Rycke[1], I. Alcaraz Aguado[1], D. Mazon[2], J. Morales[2], P. Moreau[2], G. Verdoolaege[1], and WEST Team*

[1]*Department of Applied Physics, Ghent University, Ghent, Belgium*

[2]*CEA, IRFM, F-13108 Saint-Paul-lez-Durance, France*

**See http://west.cea.fr/WESTteam/*

From current tomography to equilibrium reconstruction

Accurate knowledge of the magnetic equilibrium and kinetic profiles is essential for tokamak control and physics interpretation. Conventional equilibrium codes solve the Grad–Shafranov (GS) equation with parametrised current profiles. Bayesian methods have already been applied to equilibrium reconstruction, inferring the plasma current together with principled uncertainties on every derived quantity [1, 2]. We previously demonstrated Bayesian current tomography on WEST using external magnetics only [3], which yields robust estimates of global plasma quantities but weakly constrains the current density profile. Here we extend the framework to include *internal* diagnostics: interferometry, electron cyclotron emission (ECE), and polarimetry. We couple the resulting density and temperature profiles back into the current density reconstruction through a GS-based virtual diagnostic. The result is an integrated, self-consistent equilibrium reconstruction with full posterior uncertainties. We report results for WEST discharge **#58089 at** $t = 42.356\,\mathrm{s}$ (flat-top) and benchmark against the NICE equilibrium code [4].

Iterative Bayesian inference with internal diagnostics

Assuming toroidal symmetry, the poloidal plasma cross-section is discretised into a grid of toroidal beams of uniform current density. J_ϕ on the pixels inside the first wall is the central inferred quantity, but a means to an end: from it we obtain the poloidal flux ψ and the full equilibrium geometry, onto which the kinetic profiles n_e and T_e are mapped. Crucial for speed purposes, each diagnostic is described by a *linear* forward model $\mathbf{D} = \mathbf{F}\,\mathbf{m} + \boldsymbol{\epsilon}$, with m the inferred quantities (e.g. J_ϕ on the grid), D the measurements, F the response matrix, and ϵ zero-mean Gaussian noise with covariance Σ_D. With a Gaussian prior on m, the posterior is itself Gaussian with closed-form mean and covariance. WEST's iron core is segmented in a discrete set of current sources, with correlations modelled through a squared-exponential (SE) prior. The currents in the active and passive structures are included as Gaussian variables, so that their

contribution to the magnetic measurements is accounted for in the inference. Hyperparameters are estimated by maximising the marginal likelihood.

The reconstruction proceeds as an iterative loop:

Step 0 — external-only current. J_ϕ is inferred from pick-up coils and flux loops only, with a non-stationary conditional autoregressive (CAR) prior and a zero-current virtual observation at the first wall, yielding a first current map and flux geometry.

Step 1 — kinetic profiles. Using this flux map, n_e and T_e are inferred as 1-D profiles in normalised radius $\rho_{\mathrm{pol}} = \sqrt{\psi_N}$ (SE kernel in ρ_{pol}). Interferometry constrains n_e; ECE constrains T_e. Edge and on-axis derivative virtual observations regularise the profiles.

Step 2 — current with internal information. The profiles are turned into *virtual observations* of J_ϕ via the GS force balance,

$$J_\phi \simeq R\,\frac{\partial p}{\partial \psi} + \frac{\mu_0}{R}\,\Phi\,\frac{\partial \Phi}{\partial \psi}, \tag{1}$$

entering the inference alongside the real diagnostics, now including polarimetry (linearised by holding n_e fixed). Steps 1–2 repeat to convergence.

For the pressure term in Eq. (1) we use $p \propto (1+\alpha)\, n_e T_e$ rather than $p \propto 2 n_e T_e$, since $n_e \neq n_i$ and $T_e \neq T_i$; the scalar α absorbs $(T_i/T_e)(n_i/n_e)$ and is optimised via the marginal likelihood. The FF' contribution is currently taken from NICE. The GS virtual observation is assigned a deliberately conservative uncertainty $\epsilon_J^{EQ} = 10^5\ \mathrm{A/m^2}$ ($\sim 7\%$ of the typical WEST core current density of $\sim 1.5\ \mathrm{MA/m^2}$), guiding the reconstruction without over-constraining it [2].

Reconstruction of WEST discharge #58089

We benchmark against NICE in two configurations: external magnetics only (*NICE-ext*) and one additionally using internal interfero-polarimetry (*NICE-int*). The two bracket the role of internal information and differ markedly in the core, where J_ϕ ranges from -1.44 to $-2.15\ \mathrm{MA/m^2}$ and *NICE-int* shows the largest X-point deviation from the independent VacTH reference; we therefore compare against both rather than treating either as the true internal-current profile. Where available, the VacTH code [5] serves as an independent boundary reference. The present reconstruction and *NICE-int* are at $t = 42.356$ s; the nearest *NICE-ext* slice is at $t = 42.3683$ s

Diagnostic reconstruction errors. Table 1 reports the root-mean-square percentage error (RMSPE) between provided and reconstructed signals per diagnostic, for the present work and

both NICE configurations on a common set of valid channels. The residual is normalised by each diagnostic's maximum signal amplitude rather than channel-by-channel, since near-zero channels (notably pick-up coils) would otherwise dominate a per-channel ratio. ECE is omitted because it provides the local electron temperature directly and is not reconstructed as a signal; we use it to reconstruct T_e, but NICE does not, so no NICE-reconstructed ECE signal exists for comparison. Including polarimetry speeds up convergence and tightens the posterior.

Table 1: Root-mean-square percentage error for each set of diagnostic measurements.

Diagnostic	N_{ch}	Bayesian	*NICE-ext*	*NICE-int*
Pick-up coils	109	1.1%	0.9%	0.9%
Flux loops	4	2.0%	1.6%	1.5%
Interferometry	8	2.3%	—	3.6%
Polarimetry	7	19%	—	12%

Equilibrium scalars. The global equilibrium quantities agree well across all three reconstructions: the plasma current, magnetic axis, X-point and strike points, and the flux at the X-point all match to better than 1% e.g. $I_p = -0.4914(7)$ MA (agreeing to $\sim 0.6\%$) and the flux at the X-point to $\sim 0.1\%$. The boundary points of the present reconstruction lie closest to the independent VacTH reference, within 0.2–0.4 cm. The main difference between the NICE configurations is in the core current density, which is relevant when choosing a reference there. NICE does not provide uncertainties on these quantities, in contrast to the full posterior available here.

Current density and flux. Figure 1 shows radial and vertical cuts of J_ϕ and the poloidal flux ψ. The flux reconstruction is excellent in both cuts. The reconstructed current density reproduces the expected shape and lies between the two NICE configurations in the core: below *NICE-ext*, which uses no internal measurements, and above *NICE-int*. Note the spread between the NICE configurations here.

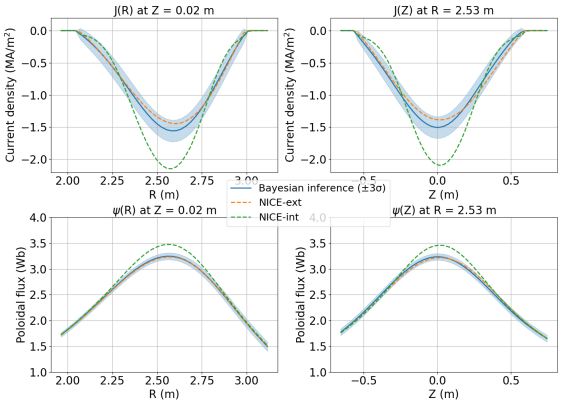

Figure 1: Radial (left) and vertical (right) cuts of J_ϕ (top) and ψ (bottom). Solid: Bayesian, $\pm 3\sigma$; dashed: NICE.

Kinetic profiles. Figures 2 and 3 show the reconstructed n_e and T_e profiles against independent WEST fitted profiles: for density, the

interferometry-based hyperbolic-tangent fit; for temperature, the ECE-based fit. The density agrees well, with a slightly weaker match in the core–edge transition. The temperature follows the expected shape but is consistently high, likely from known WEST ECE drifts and corrections [6].

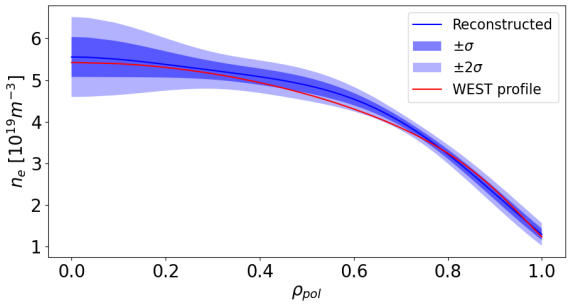

Figure 2: Electron density $n_e(\rho_{\mathrm{pol}})$. Reconstruction with $\pm\sigma/\pm2\sigma$ bands vs WEST interferometry fit.

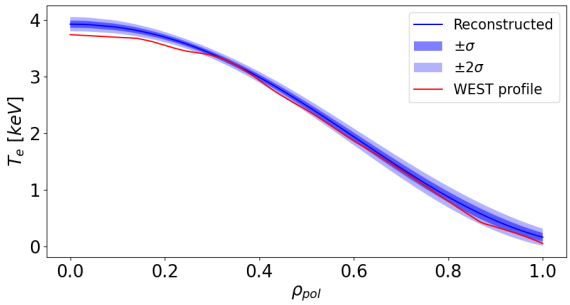

Figure 3: Electron temperature $T_e(\rho_{\mathrm{pol}})$. Reconstruction with $\pm\sigma/\pm2\sigma$ bands vs WEST ECE fit.

Conclusions and outlook

We have demonstrated an integrated Bayesian reconstruction on WEST that combines external magnetics with interferometry, ECE and polarimetry, coupled through a GS virtual diagnostic, yielding a self-consistent equilibrium and kinetic profiles with full uncertainties. Scalar equilibrium quantities show excellent agreement with those obtained by the NICE code. The reconstructed flux and the kinetic profiles also agrees well, and the internal diagnostics better constrain the core current density, where external magnetics carry little information. Planned developments include letting α vary with flux radius and infer T_i, n_i directly; infer the FF' term self-consistently; and study the GS virtual-diagnostic uncertainty more rigorously. The present scheme is split and iterative to keep each inference step linear and analytic, since the polarimetry signal ($\propto \int n_e B_{\parallel}\,\mathrm{d}l$) and the GS pressure term are nonlinear in the jointly inferred quantities; a single-step joint inference, as in the Minerva framework [2], is a natural direction.

Acknowledgements

This work is supported by the Research Foundation - Flanders (FWO) under grant 1SH6424N. The authors acknowledge the WEST team for their support.

References

[1] J. Svensson, A. Werner, *Plasma Phys. Control. Fusion* **50** (2008) 085002.
[2] S. Kwak *et al.*, *Nucl. Fusion* **62** (2022) 126069.
[3] J. De Rycke *et al.*, *JINST* **21** (2026) C04064.
[4] B. Faugeras, *Fusion Eng. Des.* **160** (2020) 112020.
[5] P. Moreau *et al.*, *Rev. Sci. Instrum.* **89** (2018) 10J109.
[6] H. Wu *et al.*, *Plasma Phys. Control. Fusion* **67** (2025) 085001.